

RELATIONSHIP BETWEEN INCREASING CME VELOCITY AT THE INITIAL STAGE OF MOTION AND CHANGE IN MAGNETIC CONDITIONS IN THE MASS EJECTION GENERATING AREA

V.G. Fainshtein 

Institute of Solar-Terrestrial Physics SB RAS,
Irkutsk, Russia, vfain@iszf.irk.ru

G.V. Rudenko 

Institute of Solar-Terrestrial Physics SB RAS,
Irkutsk, Russia, rud@iszf.irk.ru

Yu.S. Zagainova

Pushkov Institute of Terrestrial Magnetism, Ionosphere,
and Radio Wave Propagation RAS,
Troitsk, Moscow, Russia, yuliazagainova@mail.ru

Abstract. The paper is controversial since it is based on assumptions that require serious experimental confirmation. An attempt has been made to relate an increase in the coronal mass ejection (CME) velocity at the initial stage of its motion with a decrease in the free magnetic energy E_{free} in the active region. In addition, we have examined how magnetic helicity M_h changes in the active region during the selected event. We have analyzed the motion of relatively energetic halo-type CME (the CME kinetic energy is $5.2 \cdot 10^{31}$ erg) recorded on November 26, 2011 and linked to a C1.2 X-ray flare. It has been shown that when E_{free} increases with time and decreases with rising CME velocity the magnetic

helicity varies in the same way: with increasing E_{free} , M_h intensifies and vice versa. For comparison, we show E_{free} and M_h variations during the event related to an X3.1 X-ray flare and unrelated to CME. It turned out that in this case M_h intensifies during the strongest decrease in E_{free} .

Keywords: active region, coronal mass ejection, flare, free magnetic energy, magnetic helicity.

INTRODUCTION

Coronal mass ejections (CMEs) are magnetic plasma structures that are regularly erupted from the solar atmosphere into interplanetary space, carrying a significant amount of mass, energy, and magnetic flux there [Webb, Howard, 2012; Gopalswamy, 2016]. CMEs are responsible for the most severe effects of space weather on Earth, such as powerful geomagnetic storms [Baker et al., 2008]. All this determines the importance of studying CMEs, including patterns of their formation. It is currently believed that the CME energy, which can be as high as units $\cdot 10^{32}$ erg, is drawn from the solar magnetic field (see reviews [Forbes, 2000; Klimchuk, 2001]. At the same time, mechanisms of transformation of magnetic field energy into CME energy remain largely unexplained.

The presence of electric currents in the solar corona can provide free magnetic energy E_{free} in an active region (AR), which is partially transformed into CME energy and is defined as the difference between energies of given magnetic and potential fields having the same normal component at the boundary of the given volume. Calculations of E_{free} are usually based on 3D reconstruction of the coronal magnetic field using nonlinear force-free (NLFF) approximation (see, e.g., [Wheatland et al., 2000; Wiegelmann, 2004, Wiegelmann, Sakurai, 2012]. Such calculations rely on knowledge of the total photospheric magnetic field. In the NLFF approximation, the electric current is always parallel (or antiparallel) to the magnetic field vector. The most common approach to calculating the field in this approximation is the optimi-

zation method [Wheatland et al., 2000; Wiegelmann, 2004; Wiegelmann, Inhester, 2010; Rudenko, Dmitrienko, 2020].

A possible link between E_{free} change and occurrence of CME has been repeatedly analyzed. So, Metcalf et al. [2002] calculated the E_{free} change in AR when there were no solar flares in it. It was suggested that the detected rapid decrease in E_{free} was related to the generation of halo CME, although this CME was not observed in the field of view of LASCO coronagraphs. Choe, Cheng [2002] examined the relationship of a change in the force-free magnetic field with CME generation. DeVore, Antiochos [2005] calculated E_{free} for the breakout CME model [Antiochos, 1998]. Falconer, Moore, and Gary [2006], discussing magnetic causes of CME, concluded that E_{free} is preferable to magnetic twist. Lin, Kramar, and Tomczyk [2019] noted that a new approach to finding E_{free} based on tomographic measurements of solar corona parameters can be used to compare E_{free} with measured CME kinetic energy.

One of the fundamental solar magnetic field parameters is the magnetic helicity M_h [Berger, 1999]. This characteristic describes the topological properties and complexity of the field and is a quantitative characteristic of the magnetic field line twist in a selected spatial domain. An important question concerns the origin of M_h . Pevtsov, Maleev, and Longcope [2003] have found a link between a change in M_h and the emergence of a young AR. This suggests that M_h occurs in AR before its emergence.

Various aspects of the link between CME and M_h have been discussed many times. Jung et al. [2009] studied the relationship between the CME velocity V_{CME} and M_h in the regions of CME solar sources. It is shown that M_h positively correlates with V_{CME} . Zhang [2012] has concluded that CME results from magnetic helicity accumulation. Kim et al. [2013] studied magnetic helicity injection into AR that produced many flare-related CMEs. Kim et al. [2017] examined the relationship between V_{CME} and M_h near CME sources on the Sun in early phases of solar cycles 23 and 24. Pal [2022] discussed transportation of magnetic helicity into a CME magnetic flux rope.

Nonetheless, it has not been possible yet to link an increase in CME energy at the initial stage of its motion with changes in E_{free} and M_h . One of the reasons for this is that there are practically no energetic CMEs with relatively high velocity unrelated to solar flares, and very few energetic CMEs related to weak X-ray flares. In this paper, by the example of one energetic CME with a relatively high velocity associated with a C1.2 X-ray flare we have first shown that with increasing V_{CME} at the initial stage of CME motion E_{free} and M_h noticeably decrease. At the same time, before the flare and CME, E_{free} and M_h increase synchronously and relatively rapidly. A change in E_{free} during its decrease is slightly greater than the estimated maximum kinetic energy of CME at the initial stage of its motion. But if we assume that part of E_{free} is transformed into the CME magnetic field energy, the change in E_{free} during the initial CME acceleration can be comparable to the total CME energy. Note that the work is controversial as being based on assumptions that require serious experimental validation.

DATA AND METHODS

The following requirements have been formulated for the selection of events for subsequent analysis. We select CMEs recorded by Large Angle Spectrometric Coronagraph (LASCO; [Brueckner et al., 1995]) on board the Solar and Heliospheric Observatory (SOHO; [Domingo et al., 1995]) with relatively high kinetic energy, which are accompanied by very weak X-ray bursts. This is necessary in order for a change in E_{free} to depend largely on a change in CME energy, whereas the flare practically did not play a prominent role. Moreover, weak flares have a slight distortion effect on the photospheric magnetic field. This provides a more accurate calculation of E_{free} . The center of AR in which the CME occurred should not be more than 60° away in longitude from the center of the solar disk. This is necessary for the distribution of the magnetic field over AR, in which the CME appeared, to be calculated at least within ± 1 day relative to the moments of occurrence of the CME and its associated flare. We determined the CME origin from the location of the center of the CME-related flare. CMEs that meet the above requirements include halo CMEs. To select necessary events, we have used data from the LASCO CME Catalog [<https://cdaw.gsfc.nasa.gov/CME>] and the LASCO HALO CME Catalog [https://cdaw.gsfc.nasa.gov/CME_list/halo/halo.html], described in [Gopalswamy et al., 2009, 2010]. To find the desired CME, we have analyzed all halo CMEs for June 2010 – December 2023. We selected the November 26, 2011 CME event that seemed to us the most optimum in the

context of the proposed requirements with CME having a kinetic energy of $5.2 \cdot 10^{31}$ erg and a C1.2 X-ray solar flare. The analysis has shown a small number of energetic CMEs associated with weak flares. It is not surprising as it has been previously found that the relationship of V_{CME} and the CME kinetic energy E_{kin} with the intensity of flare X-rays X_{srx} or the importance of flares, recorded by GOES, features a positive trend between a change in V_{CME} or E_{kin} on the one hand and X_{srx} or flare importance on the other hand [Maričić et al., 2007; Mahrous et al., 2009; Youssef, 2013; Youssef et al., 2013; Shaltout et al., 2019].

The selected CME originated in AR NOAA 11353 and was first observed in the LASCO C2 field of view on November 26, 2011 (07:12 UT). CME with $E_{\text{kin}}=5.2 \cdot 10^{31}$ erg was related to a C1.2 X-ray flare. We can note the following facts suggesting that this CME originated in this very AR. First, using the method proposed in [Egorov, Fainshtein, 2021], we have shown that the analyzed CME appeared on the visible side of the Sun. According to [Egorov, Fainshtein, 2021], this means that the CME moves eastward in the field of view of STEREO-A COR2A and westward in the field of view of STEREO-B COR2B. This is precisely the situation that was implemented for the selected CME (Figure 1).

Secondly, it was in this AR that the CME-related solar flare with coordinates N17W49 occurred, and the halo CMEs indicated in the catalog fall into this AR (see also flare location [<https://solarmonitor.org>]). Thirdly, calculation of the direction of CME motion in 3D space from STEREO-A and -B COR data, using the method proposed in [Egorov, Fainshtein, 2021], has revealed that the continuation of the obtained direction of CME motion from low altitudes above the occulting disk of the coronagraphs to the solar surface falls into the vicinity of the said AR.

Note that, according to the catalog Near-Earth Interplanetary Coronal Mass Ejections [<https://izw1.caltech.edu/ACE/ASC/DATA/level3/icmetable2.htm>], in Earth's orbit interplanetary CME (ICME) preceded by an interplanetary shock corresponds to the CME we have selected for the analysis based on LASCO C2 data. The impact of the shock — ICME sequence on Earth's magnetosphere is accompanied by sudden commencement and generation of a minor geomagnetic disturbance.

Figure 2, *a* illustrates the CME at one of the moments of its observation in the LASCO C2 field of view; panel *b* shows the dependence of solar radiation in soft X-rays.

For the initial period of motion of the CME considered (i.e., before its appearance in the LASCO C2 field of view), we have plotted the velocity of the front part of the CME (frontal structure) as a function of time. In Figure 3, crosses mark the front fragment of the CME frontal structure for one point in time. Its lower side section is visible; the upper side one was not identified. This means that we managed to show only the southern part of the projection on the sky plane of the forepart of the frontal structure. Perhaps this is due to the motion of its selected area at an angle to the position angle of 270° to the south. The middle of the outer boundary of the CME frontal structure moves (Figure 2, *a*) in a direction with the position angle $\sim 270^\circ$.

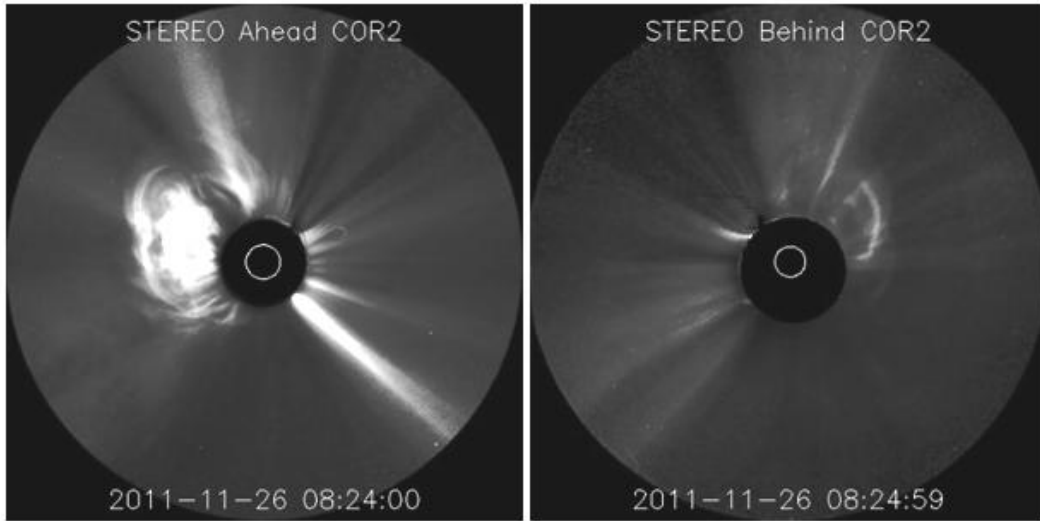


Figure 1. *a* — CME in the field of view of COR2A on board STEREO-A; *b* — CME in the field of view of COR2B on board STEREO-B (catalog [https://cdaw.gsfc.nasa.gov/stereo/daily_movies/])

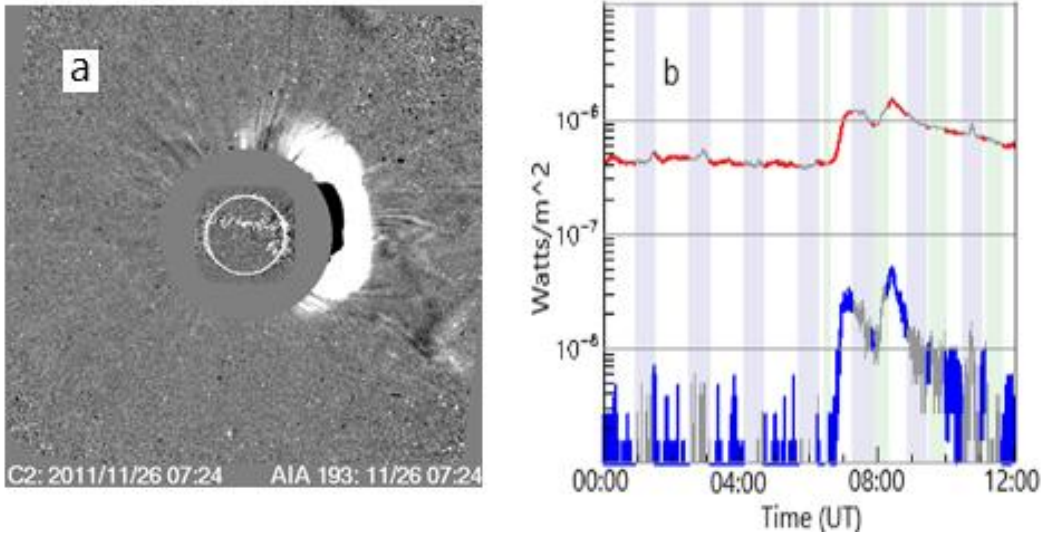


Figure 2. CME at one of the moments of its observation in the LASCO C2 field of view from the CME catalog [<https://cdaw.gsfc.nasa.gov/CME/>] (*a*) and GOES X-rays from the catalog [<https://sprg.ssl.berkeley.edu/~tohban/browser/>] (*b*). The red curve indicates the X-ray wavelength range 1–8 Å; the blue curve with gray fragments, 0.5–4 Å. On the vertical axis is the X-ray intensity (W/m^2) for any wavelength range.

To identify the outer boundary of the CME frontal structure at the initial stage of its motion, difference images of the Sun in the 171 Å channel were used which were obtained by AIA (Atmospheric Imaging Assembly) [Lemen et al., 2012] on board SDO [Pesnell et al., 2012] and were preprocessed. The preprocessing involved image normalization and overlapping. The normalization procedure was as follows. In each solar image, a quiet zone next to the analyzed AR was selected with average brightness in it. Then, for the solar image at each time point, the average brightness in the quiet region was divided by that at the first time point. Next, the brightness in each pixel of each image was multiplied by the obtained coefficients. The second procedure involved overlapping images aimed at eliminating the negative effect of the differential rotation of the Sun on identification of CME position.

A change in the CME velocity at the initial stage of motion is illustrated in Figure 4. We managed to determine it only when the CME was moving over the solar limb.

The free magnetic energy was calculated from vector measurements of the photospheric magnetic field by the Helioseismic and Magnetic Imager (HMI; [Scherrer et al., 2012]), using the approaches described in [Rudenko, Dmitrienko, 2020]. Rudenko, Dmitrienko [2020] present a post-processing method that eliminates the unavoidable magnetic field non-solenoidality calculated by optimization class codes, which is due to the noticeable role of the gas pressure gradient in the force balance at photospheric heights, as well as some mathematical properties of the optimization procedure and its associated boundary value problem. Post-processing converts the entire non-solenoidal part of the magnetic field into a solenoidal field.

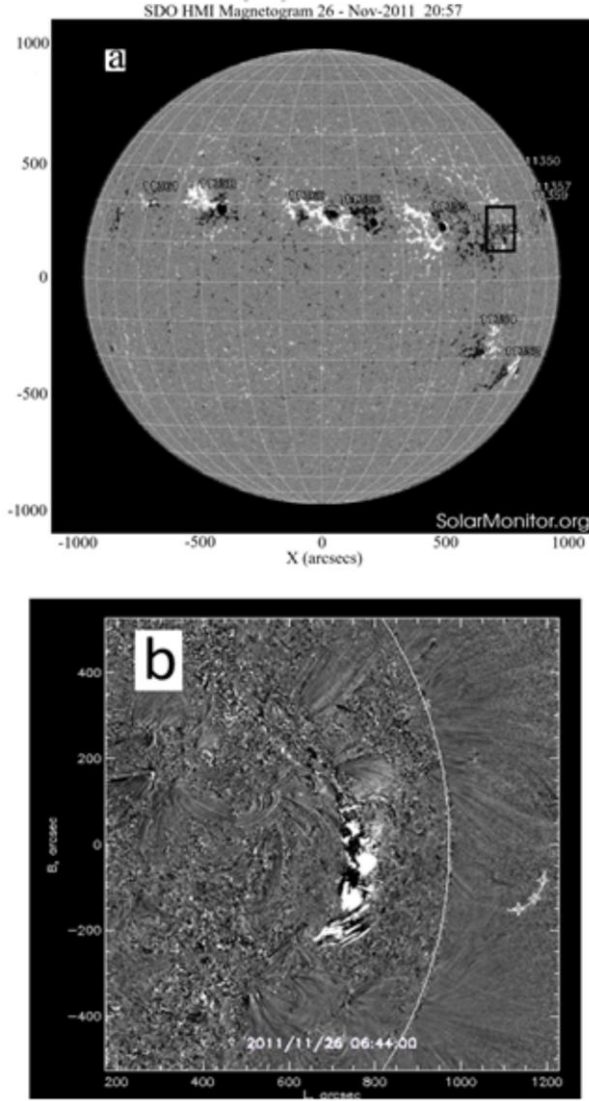


Figure 3. Magnetogram of the magnetic field measured along the line of sight with the base of the calculation box for free magnetic energy is denoted by the black rectangle (a). For the convenience of applying the base of the calculation box, we have used the magnetogram (20:57 UT) [https://solarmonitor.org] (b). An example of identification of the leading edge of CME (crosses) for 06:44:00 UT

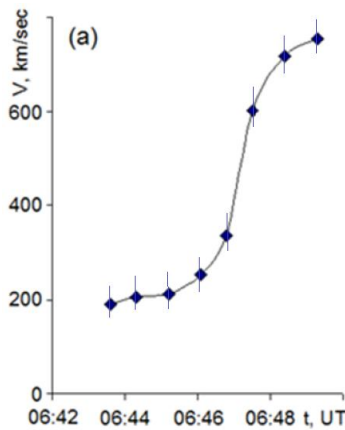


Figure 4. CME velocity as a function of time at the initial stage of motion. Error bars are estimated from the assumed shape of the frontal structure that has a small curvature

The magnetic field energy in the calculation box of volume \tilde{V}

$$E_{\text{mag}} = \frac{1}{8\pi} \int_0^{\tilde{V}} \mathbf{B}^2 dv. \quad (1)$$

Potential field energy

$$E_{\text{pot}} = \frac{1}{8\pi} \int_0^{\tilde{V}} \mathbf{B}_{\text{pot}}^2 dv. \quad (2)$$

Free magnetic energy

$$E_{\text{free}} = E_{\text{mag}} - E_{\text{pot}}. \quad (3)$$

Magnetic helicity M_h in the calculation box above AR was determined by the method described in [Rudenko, Myshyakov, 2011], which provides an algorithm for calculating the calibration-invariant helicity of the magnetic field given in the rectangular box. The algorithm was tested and verified by the well-known semi-analytical force-free field model [Low, Lou, 1990], which the authors reformulated in terms of the vector potential.

The following relations were used:

$$M_h = \int_0^{\tilde{V}} (\mathbf{A} - \mathbf{A}_{\text{pot}}) (\mathbf{B} - \mathbf{B}_{\text{pot}}) dv, \quad (4)$$

$$\mathbf{A} - \mathbf{A}_{\text{pot}} = -\frac{1}{4\pi} \int_0^{\tilde{V}} (\mathbf{r} - \mathbf{r}') / (|\mathbf{r} - \mathbf{r}'|^3 \mathbf{B}(\mathbf{r}') - \mathbf{B}_{\text{pot}}(\mathbf{r}')) dv'. \quad (5)$$

The vector \mathbf{A}_{pot} was calculated in the rectangular box by the method proposed in [Rudenko, Myshyakov, 2011].

$$\mathbf{B}_{\text{pot}} = \nabla \times \mathbf{A}_{\text{pot}}. \quad (6)$$

The magnetic field \mathbf{B}_{pot} was chosen in such a way that the normal field component \mathbf{B} at the boundary of the calculation box $S_{\tilde{V}}$ satisfied the condition

$$(\mathbf{n} \cdot \mathbf{B})_{S_{\tilde{V}}} = (\mathbf{n} \cdot \mathbf{B}_{\text{pot}})_{S_{\tilde{V}}}. \quad (7)$$

RESULTS

Figure 5 illustrates a change in E_{free} in the calculation box above AR NOAA11353. The size of the side of the base of the box was 12° ; its height, $0.22 R_s$ (R_s is the solar radius). Until $\sim 06:25$ UT, E_{free} is almost unchanged against relatively small fluctuations, then there is a sharp increase in it, which is accompanied by its abrupt decrease followed by an increase and a subsequent decrease in E_{free} . The first increase in E_{free} might have been related to a new emerging magnetic flux (NEMF) occurring on November 25, 2011 at $\sim 17:00$ UT. This NEMF ended on November 26, 2011 at $\sim 07:00$ UT. The presence of NEMF in AR NOAA11353 during the given time period is noted, for example, in Heliowiewer [https://gs671-suske.ndc.nasa.gov]. This NEMF might have been a driver of a small X-ray flare that began at nearly the same time as the first decrease in E_{free} , as well as the CME under study.

We have estimated the times $t_{1\text{free}}$ and $t_{2\text{free}}$ of the beginning and end of the first decrease in E_{free} (see Figure 5). It was found that $t_{1\text{free}}=6$ hrs 36 min, $t_{2\text{free}}=6$ hrs 48 min. It follows that $\Delta t_{\text{free}}=t_{2\text{free}}-t_{1\text{free}}=12$ min. For comparison,

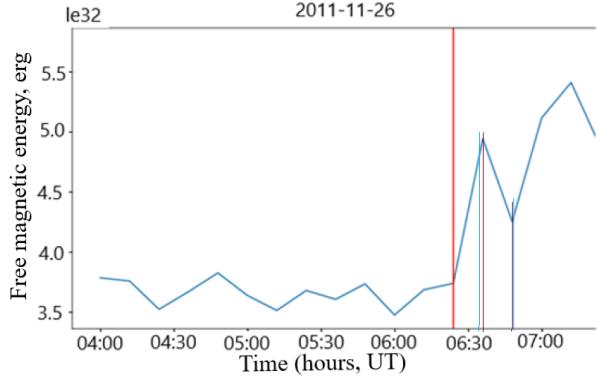


Figure 5. Variations in E_{free} in the calculation box above AR NOAA11353. The left red vertical line is the beginning of a sharp increase in E_{free} ; thin red vertical lines are the beginning and end of a decrease in E_{free} ; thin blue vertical lines are the beginning and end of the acceleration of CME at the initial stage of its motion

we also estimated the times $t_{1\text{CME}}$ and $t_{2\text{CME}}$ of the beginning and end of the rapid acceleration of the CME at the initial stage of its motion. We determined $t_{1\text{CME}}$ by extending the segment as a straight line (see Figure 4) between the first two points before intersection of this line with the horizontal time axis. The time corresponding to this point was assumed to be $t_{1\text{CME}}$. The time indicated by the last point in Figure 4 was taken as $t_{2\text{CME}}$. We have obtained the following values of $t_{1\text{CME}}$ and $t_{2\text{CME}}$: $t_{1\text{CME}} \approx 6 \text{ h } 34 \text{ min}$, $t_{2\text{CME}} \approx 6 \text{ h } 49 \text{ min}$. It follows that $\Delta t_{\text{CME}} = t_{2\text{CME}} - t_{1\text{CME}} \approx 15 \text{ min}$. Given the 12 min time resolution of the measurement of the vector photospheric magnetic field used to calculate the free energy, as well as the error in estimating $t_{1\text{CME}}$, we can hold that there is a good agreement between the beginning and end of the E_{free} decrease and the beginning and end of the rapid acceleration of the CME at the initial stage of its motion. Accordingly, the time intervals $\Delta t_{E_{\text{free}}}$ and Δt_{CME} of the decrease in E_{free} and the rapid increase in the CME velocity (kinetic energy) proved to be close.

The change in E_{free} between the beginning and the end of its decrease is $\sim 7.26 \cdot 10^{31} \text{ erg}$. The maximum kinetic energy of CME at the initial stage of its motion is equal to or slightly less than $3.47 \cdot 10^{31} \text{ erg}$ if it is supposed that the mass of the CME at the end of the initial stage of its motion is the same as in the CME catalog, or slightly smaller. E_{kin} has been estimated as in the CME catalog [https://cdaw.gsfc.nasa.gov/CME_list/], using the projection velocity. In this case, it is the projection of velocity onto the sky plane of a telescope which observes the Sun in the 171 Å channel. A more accurate estimate of E_{kin} would be to find it from the velocity in 3D space. With its ratio to the linear projected velocity $V_{3\text{D}}/V_{\text{lin}}$ for our event from the halo CME catalog, we multiply the maximum kinetic energy obtained above by $(V_{3\text{D}}/V_{\text{lin}})^2$. As a result, we get a more realistic value of $E_{\text{kin}} \leq 4.08 \cdot 10^{31} \text{ erg}$ at the end of the initial stage of CME motion. The said discrepancy between the decrease in E_{free} and the maximum kinetic energy at the initial stage of CME motion is most likely due to the fact that in addition to the kinetic energy CME receives magnetic energy, which also needs to be compensated by a

decrease in initial E_{free} . Its small part will be spent on the impulsive phase of a flare. From the change in E_{free} during its first decrease and estimated E_{kin} at the initial stage of CME motion, we can determine the probable magnetic energy of CME as $3.18 \cdot 10^{31} \text{ erg}$. As far as we know, the question about the mechanisms of the transformation of E_{free} into the CME magnetic field energy remains open.

Given that the CME mass is found with a large error and can change as the CME moves away from the solar surface (see, e.g., [Vourlidas et al., 2000; Bein et al., 2013]), it is surprising that estimated E_{kin} proved to be comparable to the change in E_{free} at the initial stage of CME motion.

How valid is it to use the mass given in the catalog [<https://cdaw.gsfc.nasa.gov/CME/>] for calculating E_{kin} at the initial stage of CME motion? A number of works (see, e.g., [Vourlidas et al., 2000; Bein et al., 2013]) have shown that the CME mass decreases slightly at shorter distances from the coronagraph's occulting disk. We therefore point out the possibility that the actual mass may be smaller than that we have selected. Although it is well known to experts that the CME mass is found with a raw error, it is employed to estimate E_{kin} and potential energy of CME in the Sun's gravity field, as well as to estimate the forces acting on CME. Since almost nothing is known about the CME mass and its change near the solar surface (see [Bein et al., 2013], where the deprojected CME mass was measured at altitudes below $3R_{\odot}$), we had no alternative to using the mass given in the CME catalog. Our estimates are valid when the selected mass is reduced to about two times. The increased difference between E_{free} and E_{kin} can be attributed to the CME magnetic field energy that may be greater than E_{kin} .

Thus, observations suggest that the time of a rapid increase in CME velocity after its occurrence approximately coincides with the time of a decrease in E_{free} from a maximum to decrease termination. Quite reasonable estimates of the maximum CME kinetic energy during the rapid increase in its velocity have shown that a change in E_{free} during its first decrease (see Figure 5) roughly agree with the sum of the maximum CME kinetic energy during the sharp increase in its velocity and the expected CME magnetic field energy at the end of the increase in its velocity.

Nevertheless, note the following. It appeared that for several time points for which the CME velocity was measured (see Figure 4), the frontal structure proved to be higher than the height of the box in which E_{free} was calculated. How can this affect the results? Let us try to estimate how the dependence $E_{\text{free}}(t)$ will look like if the height of the calculation box includes all points of measured V_{CME} , i.e. it increases. If a decrease in E_{free} really coincides with a change in the CME energy at the initial stage of its motion, the beginning and end of the decrease in $E_{\text{free}}(t)$ will not change since they are determined by the beginning and end of CME acceleration at the initial stage of motion. At the same time, the beginning and end of the $E_{\text{free}}(t)$ decrease will rise, but to a small height because the density of $E_{\text{free}}(t)$ decreases with height. If we are not mistaken in estimating the total energy of the CME at the initial stage of its motion,

the decrease in $E_{\text{free}}(t)$ will not change, but the decrease will begin and end at other values of $E_{\text{free}}(t)$. If we are mistaken in estimating the total energy of the CME at the initial stage of its motion by underestimating the CME magnetic field energy, the beginning of the decrease in $E_{\text{free}}(t)$ will go to a larger height. However, the data analysis method will generally remain the same. Thus, the exit of measuring points of CME velocity from the computational domain may lead to underestimation of the CME magnetic field energy, yet will not affect the moments of the beginning and end of the $E_{\text{free}}(t)$ decrease when the height of the box for calculating $E_{\text{free}}(t)$ changes.

The proximity of the estimated time it takes of the maximum CME velocity at the initial stage of its motion to reach the time resolution (12 min) of HMI vector magnetic field measurements may seem strange, which casts some doubt on the reliability of the results. In fact, the time for CME to reach its maximum speed at the initial stage of its motion is quite possible. This is confirmed by repeated measurements of $V_{\text{CME}}(t)$ after the occurrence of CME (see, for example, $V_{\text{CME}}(t)$ [Temmer et al., 2010]). For the June 03, 2007 event, the time of a sharp increase in V_{CME} to the maximum value $dT \sim 8$ min; and for the December 31, 2007 event, $dT \sim 13$ min.

There are events for which the calculated time of change in E_{free} during a solar flare almost exactly coincides with the time resolution of the HMI vector magnetic field measurements. This is shown, for example, for two powerful X-ray flares recorded on September 06, 2017 ([McKevitt et al., 2024], see Figure 3). For the October 24, 2014 event shown below (Figure 6), the total time of E_{free} change was 36 min, but the main E_{free} change occurred for 12 min.

Note that an increase in E_{free} in AR before eruptive processes (flares, CMEs) is fairly common. At the same time, the time scales of such an increase vary widely. This is shown, for instance, in [Sun et al., 2012] for the February 15, 2011 event: a rapid increase lasted for ~ 2 –3 hrs, followed by a slow increase for ~ 2 days. This event features an X2.2 X-ray flare and CME with $E_{\text{kin}} = 9.7 \cdot 10^{30}$ erg., i.e. this is the case with a strong flare and a relatively weak CME. McKevitt et al. [2024] have shown an E_{free} change that accompanied two eruptive events on September 06, 2017. In the first event, an X2.2

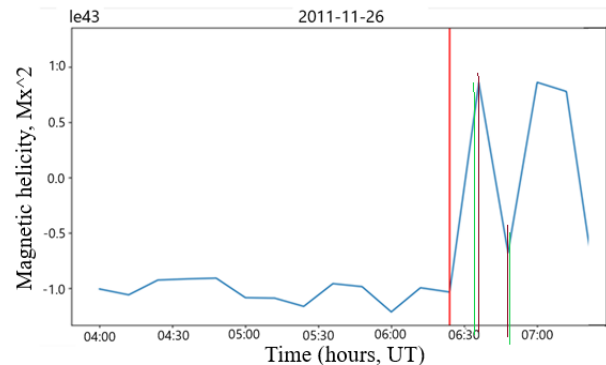


Figure 6. Time variation in magnetic helicity for the November 26, 2011 event. Vertical lines are the same as in Figure 5

X-ray flare with weak CME was recorded; in the second event, an X9.3 flare and a fairly powerful CME with $E_{\text{kin}} = 3.6 \cdot 10^{32}$ erg. Before the former event, E_{free} increased for at least 3 hrs (the authors of the cited article failed to show the entire interval of E_{free} change before the beginning of its decrease); before the latter, ~ 3 hrs. The rapid increase in E_{free} for a few minutes in our case is most likely due to the peculiarities of the NEMF behavior.

Let us try to explain features of the E_{free} behavior after the end of its first decrease. It is clear that the change in $E_{\text{free}}(t)$ during this period weakly reflects the evolution of the CME. According to the catalog [https://cdaw.gsfc.nasa.gov/CME_list/halo/halo.html], after a rapid initial acceleration $V_{\text{CME}}(t)$ changes rather slowly. This means that the kinetic energy also changes slowly, without abrupt changes that could explain the second sharp decrease in $E_{\text{free}}(t)$. The abrupt increase in $E_{\text{free}}(t)$ after its first decrease can be attributed to the continuation of NEMF, which stops at $\sim 07:00$ UT, and the low consumption of free energy by the flare and CME during this period. After that, $E_{\text{free}}(t)$ continues to increase for ~ 12 min, but at a slower rate. The subsequent decrease in E_{free} represents the termination of the new emerging magnetic flux, $E_{\text{free}}(t)$ decreases to approximately the value at the beginning of the V_{CME} increase (the first maximum of $E_{\text{free}}(t)$).

Figure 6 illustrates a change in $M_h(t)$ for the November 26, 2011 event. Conspicuous is the correspondence between changes in $E_{\text{free}}(t)$ and $M_h(t)$: an increase in $E_{\text{free}}(t)$ is accompanied by an increase in $M_h(t)$ and vice versa. A slight change in $E_{\text{free}}(t)$ before the beginning of its first increase occurs with a slight change in $M_h(t)$.

Note that such a correspondence between the behavior of $E_{\text{free}}(t)$ and $M_h(t)$ is not typical of all eruptive events. Figure 7, *a* exhibits a powerful flare that occurred on October 24, 2014; Figure 6, *b* illustrates a change in $E_{\text{free}}(t)$ for the eruptive event on October 24, 2014, representing an X3.1 solar flare unrelated to CME. Various aspects of this event and several other similar ones (a powerful X-ray flare unrelated to CME) have been discussed in detail in [Thalmann et al., 2015]. Figure 7, *b* shows a change in $M_h(t)$ for this event. It is apparent that during the fastest decrease in $E_{\text{free}}(t)$ $M_h(t)$ increases. Before and after the end of the eruptive event, $E_{\text{free}}(t)$ and $M_h(t)$ change with time in antiphase, on average.

The fact that $E_{\text{free}}(t)$ and $M_h(t)$ can change synchronously was established for the June 07, 2011 eruptive event [Egorov et al., 2020]. It included a powerful CME with $E_{\text{kin}} = 1.8 \cdot 10^{32}$ erg, an M2.5 flare, and eruption of a relatively large filament. Comparison between changes in $E_{\text{free}}(t)$ and $M_h(t)$ (see Figures 7, 12, top and bottom right panels in the cited work) for part of AR, where the magnetic field changed most strongly during the eruptive event, reveals a similarity between the changes in $E_{\text{free}}(t)$ and $M_h(t)$.

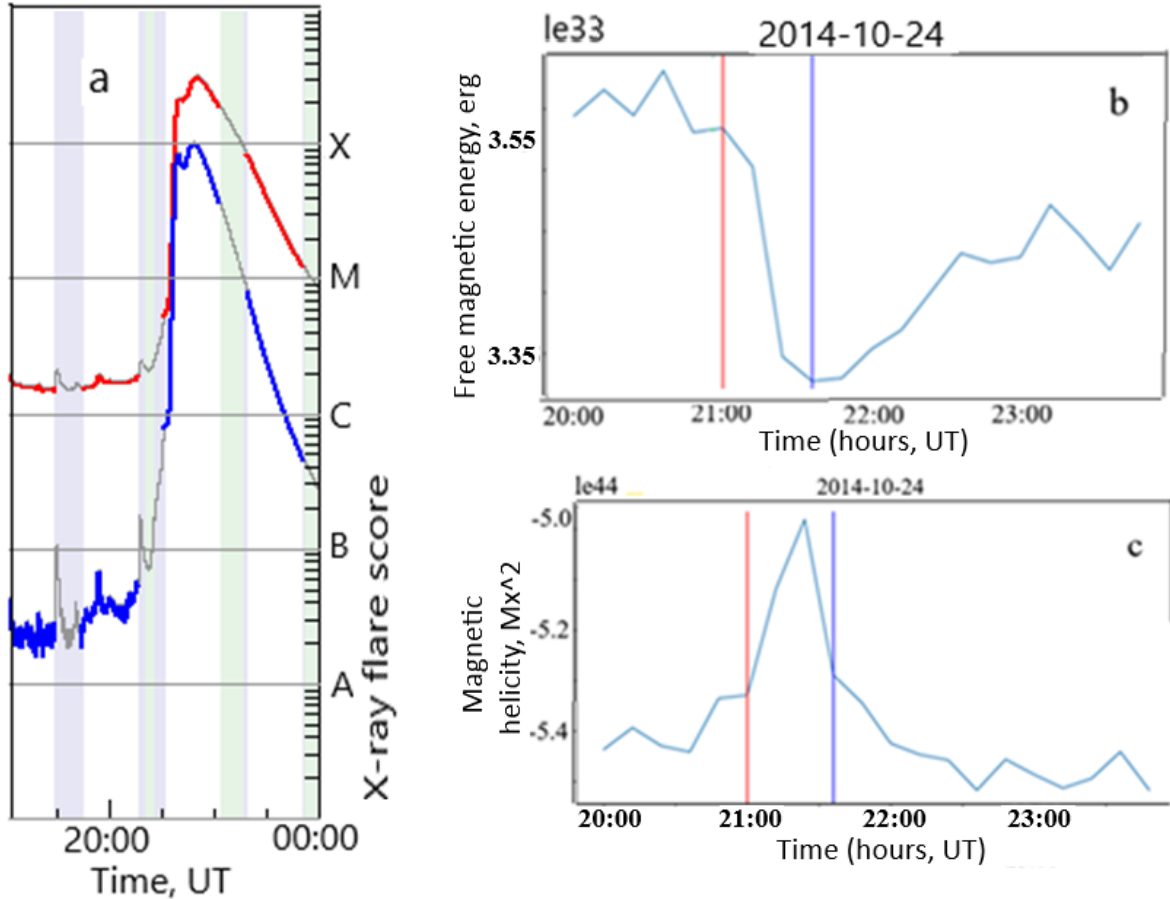


Figure 7. Intensity of soft X-rays (a) during an X3.1 solar flare from the catalog [<https://sprg.ssl.berkeley.edu/~tohban/browser/>] (upper line is the wavelength range 1–8 Å; lower line, 0.5–4 Å); change in $E_{\text{free}}(t)$ (b); change in $M_h(t)$ (c). The left vertical line indicates the beginning of a decrease in E_{free} close to the beginning of an increase in the flare emission intensity. The right vertical line is the time close to the moment when E_{free} stopped decreasing.

CONCLUSION

The occurrence of CME is a fast process in the lower solar corona, which is accompanied by a release of a large amount of energy that can be as high as $(2\div 3)\cdot 10^{25}$ J. It has been repeatedly suggested that the source of this energy is the free magnetic energy E_{free} accumulated in the active region in which the CME originated. But it has not yet been possible to demonstrate this convincingly. One of the reasons for this is that CME is accompanied by solar flares, which are followed by a decrease in E_{free} . In many cases, it is impossible to distinguish the E_{free} change related to the occurrence of CME from the E_{free} change driven by a solar flare. For this purpose, we should select a CME with relatively high E_{kin} associated with a very weak flare. However, it is quite difficult to select such an event since on average with an increase in CME E_{kin} the intensity of soft X-rays of the associated flare increases. We managed to find one event for 2010–2023 that meets this requirement. We chose a halo CME with relatively high $E_{\text{kin}}=5.2\cdot 10^{31}$ erg linked to a C1.2 X-ray flare. The CME was first detected in the LASCO C2 field of view on November 26, 2011 (07:12 UT). We assumed that a driver of this CME and the flare was a new emerging magnetic flux.

We have shown that an increase in CME velocity at the initial stage of its motion almost concurs with a decrease in $E_{\text{free}}(t)$, i.e. an increase in CME velocity begins approximately at the moment when E_{free} begins to decrease, and ends approximately at the moment of the end of its decrease. The change in the total CME energy is close, according to estimates, to the change in $E_{\text{free}}(t)$ during its decrease.

For the event considered, we have compared the behavior of $E_{\text{free}}(t)$ and $M_h(t)$. Changes in $E_{\text{free}}(t)$ and $M_h(t)$ proved to have the same trends: an increase in $E_{\text{free}}(t)$ is accompanied by an increase in $M_h(t)$ and vice versa. This trend is unnecessary for all eruptive events. We compared the behavior of $E_{\text{free}}(t)$ and $M_h(t)$ for an eruptive event that was an X3.1 X-ray flare unrelated to CME. The flare was recorded on October 24, 2014. For such an event, $E_{\text{free}}(t)$ and $M_h(t)$ during the fastest decrease in E_{free} , as well as before and after the eruptive event, change on average in the opposite way: if $E_{\text{free}}(t)$ decreases, $M_h(t)$ increases and vice versa.

When analyzing the selected event, we had to make several assumptions. For example, we assumed that the CME mass at the end of the initial stage of its motion was equal to or slightly smaller than the mass given in the CME catalog. We also supposed that a decrease in

$E_{\text{free}}(t)$ in the calculation box may be linked to a change in the CME velocity even when it is above the calculation box at a relatively low altitude. All this stimulates the continuation of the research aimed at finding a link between changes in $E_{\text{free}}(t)$ and V_{CME} at the initial stage of CME motion.

The work was financially supported by of the Ministry of Science and Higher Education of the Russian Federation.

We are grateful to the LASCO/SOHO, HMI/SDO, AIA/SDO, STEREO COR2A, COR2B, and GOES teams for providing free access to the data. We also express our gratitude to creators of the catalogs [https://cdaw.gsfc.nasa.gov/CME_list/index.html] and [https://cdaw.gsfc.nasa.gov/CME_list/halo/halo.html] for providing access to their data. Rudenko G.V. thanks the Irkutsk Supercomputing Center of the Siberian Branch of the Russian Academy of Sciences for providing access to the HPC cluster "Academician V.M. Matrosov" (Irkutsk Supercomputing Center SB RAS, IDSTU SB RAS [<http://hpc.icc.ru>])

REFERENCES

- Antiochos S.K. The Magnetic Topology of Solar Eruptions. *Astrophys. J.* 1998, vol. 502, iss. 2, pp. L181–L184. DOI: [10.1086/311507](https://doi.org/10.1086/311507).
- Baker D.N., Balstad, R., Bodeau, J.M., and 15 more co-authors. *Severe Space Weather Events — Understanding Social and Economic Impacts: A Workshop Rep.* The National Academies Press, Washington DC. 2008.
- Bein B.M., Temmer M., Vourlidis A., et al. The height evolution of the “true” coronal mass ejection mass derived from stereo COR1 and COR2 observations. *Astrophys. J.* 2013, vol. 768:31, 12 p. DOI: [10.1088/0004-637X/768/1/31](https://doi.org/10.1088/0004-637X/768/1/31).
- Berger M.A. Introduction to magnetic helicity. *Plasma Physics and Controlled Fusion*. 1999, vol. 41, pp. B167–B175. DOI: [10.1088/0741-3335/41/12B/312](https://doi.org/10.1088/0741-3335/41/12B/312).
- Brueckner G.E., Howard R.A., Koomen M.J., et al. The Large Angle Spectroscopic Coronagraph (LASCO). *Solar Phys.* 1995, vol. 162, pp. 357–402. DOI: [10.1007/BF00733434](https://doi.org/10.1007/BF00733434).
- Choe G.S., Cheng C.Z. Energy of Force-free Magnetic Fields in Relation to Coronal Mass Ejections. *Astrophys. J.* 2002, vol. 574, iss. 2, pp. L179–L182. DOI: [10.1086/342478](https://doi.org/10.1086/342478).
- DeVore R.C., Spiro A.K. Magnetic free energies of breakout coronal mass ejections. *Astrophys. J.* 2005, vol. 628, iss. 2, pp. 1031–1045. DOI: [10.1086/431141](https://doi.org/10.1086/431141).
- Domingo V., Fleck B., Poland A.I. The SOHO mission: an overview. *Solar Phys.* 1995, vol. 162, pp. 1–37. DOI: [10.1007/BF00733425](https://doi.org/10.1007/BF00733425).
- Egorov Ya.I., Fainshtein V.G. A simple technique for identifying the propagation direction of CME in a 3^d space. *Solar Phys.* 2021, vol. 296, iss. 11, article id. 161. DOI: [10.1007/s11207-021-01904-3](https://doi.org/10.1007/s11207-021-01904-3).
- Egorov Y.I., Fainshtein V.G., Myshyakov I.I., et al. Studying magnetic field variations accompanying the 2011 June 7 eruptive event, by using nonlinear force-free field modeling. *Solar Phys.* 2020, vol. 295, iss. 4, article id. 52. DOI: [10.1007/s11207-020-01613-3](https://doi.org/10.1007/s11207-020-01613-3).
- Falconer D.A., Moore R.L., Gary G.A. Magnetic causes of solar coronal mass ejections: dominance of the free magnetic energy over the magnetic twist alone. *Astrophys. J.* 2006, vol. 644, iss. 2, pp. 1258–1272. DOI: [10.1086/503699](https://doi.org/10.1086/503699).
- Forbes T.G. A review on the genesis of coronal mass ejections. *J. Geophys. Res.* 2000, vol. 105, pp. 23153–23166. DOI: [10.1029/2000JA000005](https://doi.org/10.1029/2000JA000005).
- Gopalswamy N. History and development of coronal mass ejections as a key player in solar terrestrial relationship. *Geoscience Lett.* 2016, vol. 3, article id. 8, 18 p. DOI: [10.1186/s40562-016-0039-2](https://doi.org/10.1186/s40562-016-0039-2).
- Gopalswamy N., Yashiro S., Michalek G., et al. The SOHO/LASCO CME catalog. *Earth, Moon, and Planets.* 2009, vol. 104, pp. 295–313. DOI: [10.1007/s11038-008-9282-7](https://doi.org/10.1007/s11038-008-9282-7).
- Gopalswamy N., Yashiro S., Michalek G., et al. A catalog of halo coronal mass ejections from SOHO. *Sun and Geosphere.* 2010, vol. 5, pp. 7–16.
- Howard T. Coronal Mass Ejections: An Introduction. *Astrophysics and Space Science Library.* 2011, vol. 376. Springer Science+Business Media, LLC, DOI: [10.1007/978-1-4419-8789-1](https://doi.org/10.1007/978-1-4419-8789-1).
- Jung H., Gopalswamy N., Akiyama S., Yashiro S. Relation between magnetic helicity and CME speed in source active regions. *American Geophysical Union, Fall Meeting.* 2009, abstract id.SH41B-1669.
- Kim R.-S., Park S.-H., Jang S., et al. Relation of CME speed and magnetic helicity in CME source regions on the Sun during the early phase of solar cycles 23 and 24. *Solar Phys.* 2017, vol. 292, iss. 4, article id. 66, 14 p. DOI: [10.1007/s11207-017-1079-2](https://doi.org/10.1007/s11207-017-1079-2).
- Klimchuk J.A. *Space Weather (Geophysical Monograph 125)*. Washington: American Geophys. Union, 2001, 143 p. DOI: [10.1029/GM125p0143](https://doi.org/10.1029/GM125p0143).
- Lemen J.R., Title A.M., Akin D.J., et al. The Atmospheric Imaging Assembly (AIA) on the Solar Dynamics Observatory (SDO). *Solar Phys.* 2012, vol. 275, pp. 17–40. DOI: [10.1007/s11207-011-9776-8](https://doi.org/10.1007/s11207-011-9776-8).
- Lin H., Kramar M., Tomczyk S. Tomographic measurements of magnetic free energy in CME source regions. *American Geophysical Union, Fall Meeting 2019*. Abstract #SH53B-3378. 2019.
- Low B.C., Lou Y.Q. Modeling solar force-free magnetic fields. *Astrophys. J.* 1990, vol. 352, p. 343. DOI: [10.1086/168541](https://doi.org/10.1086/168541).
- Mahrous A., Shaltout M., Beheary M.M., et al. CME–flare association during the 23rd solar cycle. *Adv. Space Res.* 2009, vol. 43, iss. 7, pp. 1032–1035. DOI: [10.1016/j.asr.2009.01.028](https://doi.org/10.1016/j.asr.2009.01.028).
- Maričić D., Vršnak B., Stanger A.L., et al. Acceleration phase of coronal mass ejections: II. Synchronization of the energy release in the associated flare. *Solar Phys.* 2007, vol. 241, pp. 99–112. DOI: [10.1007/s11207-007-0291-x](https://doi.org/10.1007/s11207-007-0291-x).
- Metcalf T.R., Mickey D.L., Labonte B.J., Ryder L.A. The Magnetic free energy and a CME in active region 8299. 2002. *Multi-Wavelength Observations of Coronal Structure and Dynamics — Yohkoh 10th Anniversary Meeting. Proc. September 17–20, 2001, Hawaii, USA*. Published by Elsevier Science on behalf of COSPAR in the COSPAR Colloquia Ser. P. 249.
- McKevitt J., Jarolim R., Matthews S., et al. The link between non-thermal velocity and free magnetic energy in solar flares. *Astrophys. J. Lett.* 2024, vol. 961, iss. 2, id. L29, 7 p. DOI: [10.3847/2041-8213/ad1bee](https://doi.org/10.3847/2041-8213/ad1bee).
- Pal Sanchita. Uncovering the process that transports magnetic helicity to coronal mass ejection flux ropes. *Adv. Space Res.* 2022, vol. 70, iss. 6, pp. 1601–1613. DOI: [10.1016/j.asr.2021.11.013](https://doi.org/10.1016/j.asr.2021.11.013).
- Pesnell W.D., Thompson B.J., Chamberlin P.C. The Solar Dynamics Observatory (SDO). *Solar Phys.* 2012, vol. 275, pp. 3–15. DOI: [10.1007/s11207-011-9841-3](https://doi.org/10.1007/s11207-011-9841-3).
- Pevtsov A.A., Maleev V.M., Longcope D.W. Helicity evolution in emerging active regions. *Astrophys. J.* 2003, vol. 593, pp. 1217–1225. DOI: [10.1086/376733](https://doi.org/10.1086/376733).
- Rudenko G.V., Myshyakov I.I. Gauge-invariant helicity for force-free magnetic fields in a rectangular box. *Solar Phys.* 2011, vol. 270, iss. 1, article id. 165. DOI: [10.1007/s11207-011-9743-4](https://doi.org/10.1007/s11207-011-9743-4).

- Rudenko G.V., Dmitrienko I.S. Validity of nonlinear force-free field optimization reconstruction. *Solar Phys.* 2020, vol. 295, iss. 6, article id. 85. DOI: [10.1007/s11207-020-01647-7](https://doi.org/10.1007/s11207-020-01647-7).
- Scherrer P.H., Schou J., Bush R.I., et al. The Helioseismic and Magnetic Imager (HMI) investigation for the Solar Dynamics Observatory (SDO). *Solar Phys.* 2012, vol. 275, pp. 207–227. DOI: [10.1007/s11207-011-9834-2](https://doi.org/10.1007/s11207-011-9834-2).
- Shaltout Abdelrazek M.K., Amin Eid A., Beheary M.M., Hamid R.H. A statistical study of CME-associated flare during the solar cycle 24. *Adv. Space Res.* 2019, vol. 63, pp. 2300–2311. DOI: [10.1016/j.asr.2018.12.022](https://doi.org/10.1016/j.asr.2018.12.022).
- Sun X., Hoeksema J.T., Liu Y., et al. Evolution of magnetic field and energy in a major eruptive active region based on SDO/HMI observation. *Astrophys. J.*, 2012, vol. 748, article id. 77, 15 p.
- Sung-Hong Park, Kanya Kusano, Kyung-Suk Cho, Jongchul Chae, Su-Chan Bong, Pankaj Kumar, et al. Study of magnetic helicity injection in the active region NOAA 9236 producing multiple flare-associated coronal mass ejection events. *Astrophys. J.*, 2013, vol. 778, iss. 1, article id. 13, 8 p.
- Temmer M., Veronig A.M., Kontar E.P., et al. Combined STEREO/RHESSI study of coronal mass ejection acceleration and particle acceleration in solar flares. *Astrophys. J.* 2010, vol. 712, no. 2, pp. 1410–1420. DOI: [10.1088/0004-637X/712/2/1410](https://doi.org/10.1088/0004-637X/712/2/1410).
- Thalmann J.K., Su, Y. Temmer M., Veronig A.M. The confined X-class flares of solar active region 2192. *Astrophys. J. Lett.* 2015, vol. 801, no. L23, 5 p. DOI: [10.1088/2041-8205/801/2/L23](https://doi.org/10.1088/2041-8205/801/2/L23).
- Vourlidas A., Subramanian P., Dere K.P., Howard R.A. Large-angle spectrometric coronagraph measurements of the energetics of coronal mass ejections. *Astrophys. J.* 2000, vol. 534, pp. 456–467. DOI: [10.1086/308747](https://doi.org/10.1086/308747).
- Webb D.F., Howard T.A. Coronal mass ejections: Observations. *Living Rev. in Solar Phys.* 2012, vol. 9, iss. 1, article id. 3, 83 p. DOI: [10.12942/lrsp-2012-3](https://doi.org/10.12942/lrsp-2012-3).
- Wheatland M.S., Sturrock P.A., Roumeliotis G. An optimization approach to reconstructing force-free fields. *Astrophys. J.* 2000, vol. 540, pp. 1150–1155. DOI: [10.1086/309355](https://doi.org/10.1086/309355).
- Wiegelmann T. Optimization code with weighting function for the reconstruction of coronal magnetic fields. *Solar Phys.* 2004, vol. 219, pp. 87–108. DOI: [10.1023/B:SOLA.0000021799.39465.36](https://doi.org/10.1023/B:SOLA.0000021799.39465.36).
- Wiegelmann T., Inhester B. How to deal with measurement errors and lacking data in nonlinear force-free coronal magnetic field modelling? *Astron. Astrophys.* 2010, vol. 516, id. A107, 5 p. DOI: [10.1051/0004-6361/201014391](https://doi.org/10.1051/0004-6361/201014391).
- Wiegelmann T., Sakurai T. Solar force-free magnetic fields. *Living Rev. Solar Phys.* 2012, vol. 9, article id. 5, 49 p. DOI: [10.12942/lrsp-2012-5](https://doi.org/10.12942/lrsp-2012-5).
- Youssef M. Statistical study of the CME solar flares associated events. *Earth, Moon, and Planets.* 2013, vol. 110, pp. 185–105. DOI: [10.1007/s11038-013-9419-1](https://doi.org/10.1007/s11038-013-9419-1).
- Youssef M., Mawad R., Shaltout Mosalam. A statistical study of post-flare associated CME events. *Adv. Space Res.* 2013, vol. 51, pp. 1221–1229. DOI: [10.1016/j.asr.2012.10.007](https://doi.org/10.1016/j.asr.2012.10.007).
- Zhang M. Coronal mass ejection as a result of magnetic helicity accumulation. *Hinode-3: The 3rd Hinode Science Meeting, Proc.* 1–4 December 2009, Tokyo, Japan. ASP Conference Ser. Vol. 454. San Francisco: Astronomical Society of the Pacific. 2012, p. 399. DOI: [10.1007/s11207-011-9834-2](https://doi.org/10.1007/s11207-011-9834-2).
URL: <https://solarmonitor.org> (accessed April 15, 2025).
URL: https://cdaw.gsfc.nasa.gov/stereo/daily_movies (accessed April 15, 2025).
URL: <https://cdaw.gsfc.nasa.gov/CME> (accessed April 15, 2025).
URL: https://cdaw.gsfc.nasa.gov/CME_list/halo/halo.html (accessed April 15, 2025).
URL: <https://sprg.ssl.berkeley.edu/~tohban/browser/> (accessed April 15, 2025).
URL: <https://izw1.caltech.edu/ACE/ASC/DATA/level3/icmetable2.htm> (accessed April 15, 2025).
URL: https://cdaw.gsfc.nasa.gov/CME_list/index.html (accessed April 15, 2025).
URL: <https://gs671-suske.ndc.nasa.gov> (accessed April 15, 2025).
URL: https://cdaw.gsfc.nasa.gov/CME_list/ (accessed April 15, 2025).

Original Russian version: Fainshtein V.G., Rudenko G.V., Zagainova Yu.S., published in *Solnechno-zemnaya fizika*. 2025, vol. 11, no. 2, pp. 5–14. DOI: [10.12737/szf-112202501](https://doi.org/10.12737/szf-112202501). © 2025 INFRA-M Academic Publishing House (Nauchno-Izdatelskii Tsentr INFRA-M).

How to cite this article

Fainshtein V.G., Rudenko G.V., Zagainova Yu.S. Relationship between increasing CME velocity at the initial stage of motion and change in magnetic conditions in the mass ejection generating area. *Sol.-Terr. Phys.* 2025, vol. 11, iss. 2, pp. 3–11. DOI: [10.12737/stp-112202501](https://doi.org/10.12737/stp-112202501).